Automated Integration of Multi-Slice Spatial Transcriptomics Data in 2D and 3D

Denis Bienroth[1,†], Natalie Charitakis[1,2,†], Dillon Wong [1,3], Sabrina Jaeger-Honz[4] Dimitar Garkov[4], Kevin I. Watt[1,7], Julian Stolper[1,2], Hazel Chambers-Smith[5], Duncan MacGregor[5], Bronwyn Christiansen[5], Adam T. Piers[1,6], Enzo R. Porrello[1,6,7^], David A. Elliott[1,7^], Karsten Klein[4,^], Hieu T. Nim[1,2,8,^], Falk Schreiber[3,4,9*], and Mirana Ramialison[1,2,8,*]

1 Novo Nordisk Foundation Center for Stem Cell Medicine, Murdoch Children's Research Institute, Parkville, Victoria, 3052, Australia.

2 Department of Paediatrics, Faculty of Medicine, Dentistry & Health Sciences, University of Melbourne, Melbourne 3010, Australia.

3 School of Computing and Information Systems, Faculty of Engineering and Information Technology, University of Melbourne, Parkville

4 Department of Computer and Information Science, University of Konstanz, Konstanz, 78464, Germany

5 Anatomical Pathology, The Royal Children's Hospital, Melbo urne, Victoria, 3052, Australia

6 Melbourne Centre for Cardiovascular Genomics and Regenerative Medicine, The Royal Children's Hospital, Melbourne, Victoria, 3052, Australia

7 Department of Anatomy and Physiology, University of Melbourne, Parkville, Victoria, 3052, Australia

8 Australian Regenerative Medicine Institute, System Biology Institute, Monash University, Clayton, Melbourne, Victoria, 3168, Australia

9 Faculty of Information Technologies, Monash University, Melbourne, Victoria, 3168, Australia

†: co-first authors

^: co-senior authors

*: co-corresponding authors

Falk Schreiber: Falk.Schreiber@uni-konstanz.de

Mirana Ramialison: Mirana.Ramialison@mcri.edu.au

ABSTRACT

The field of spatial transcriptomics is rapidly evolving, with increasing sample complexity, resolution, and tissue size. Yet the field lacks comprehensive solutions for automated integration and analysis of multi-slice data in either stacked (3D) or co-planar (2D) formation. To address this, we developed VR-Omics, a free, platform-agnostic software that distinctively provides end-to-end automated processing of multi-slice data through a biologist-friendly interface. Benchmarking against existing methods demonstrates VR-Omics' unique strengths to perform comprehensive end-to-end analysis of multi-slice stacked data. Applied to rare paediatric cardiac rhabdomyomas, VR-Omics uncovered previously undetected dysregulated metabolic networks through co-planar slice analysis, demonstrating its potential for biological discoveries.

BACKGROUND

Spatial transcriptomics (ST) is a rapidly evolving technology allowing the capture of spatial gene expression at unprecedented resolution to advance our comprehension of cellular processes and molecular mechanisms [1, 2]. Since many tissue samples being profiled exceed a standard vendor-provided chip size, analysing multi-slice ST data is an important task that cannot be fully supported using current single-slice tools [3]. Multi-slice samples are typically co-planar, where slices lie on the same plane (*e.g.* twelve prostate cryosections sections [4]) or 3D stacked, where parallel slices are orthogonally adjacent (*e.g.* thirteen E16.5 mouse embryo sections [5]). Bridging this technical gap enables tissues to be studied in their complete native spatial context, providing crucial insights, and understanding of the tissue structure and characteristics.

Several ST algorithms have been developed to process and mine ST multi-slice data, including Stitch3D [6] and VT3D [7]. However, these specialised multi-slice pipelines or analytical programmes handle only a narrow scope within the end-to-end analysis pipeline while also requiring advanced computational skills, creating a substantial barrier for end-users. Several online portals allow viewing of existing multi-slice ST datasets (SpatialDB [8], STOmicsDB [9], SODB [10], SOAR [11]) but limit the user to the datasets that are publicly available and do not allow analyses of user-uploaded multi-slice data. Finally, no current multi-slice ST tools allow manual interactive alignment of multi-slice data, both co-planar and 3D stacked formations, providing an interactive graphical user interface.

Here we present VR-Omics, an interactive, end-to-end platform to process, analyse and visualise ST data, all through a user-friendly graphical user interface (GUI). VR-Omics is designed to democratize ST data analysis, making it accessible to both bioinformaticians and non-bioinformaticians while generating reproducible results in a timesaving manner. As inputs, VR-Omics supports data from both sequencing and imaging-based ST technologies, as well as custom ST data matrices [12-14]. VR-Omics primarily functions as a conventional desktop application, with the inclusion of VR integration as an optional supplementary feature. While fully supporting single-slice ST data, VR-Omics further facilitates multi-slice ST data with additional capabilities, including merging or manual alignment of slides and comprehensive 3D visualisation.

We demonstrate the utility of VR-Omics through the analysis of both single and multi-slice rare paediatric cardiac rhabdomyomas (cRMs) for which the disease mechanism remains unknown [15, 16]. Using VR-omics, we identified novel transcriptional signatures distributed in discrete niches across the cRM. Additionally, we showcased the precision of VR-Omics by

performing a meticulous three-dimensional (3D) reconstruction of cardiac structures, rigorously validating its performance against state-of-the-art ST tools. These multifaceted use-cases collectively exemplify the versatility and robustness of VR-Omics as a pivotal tool for effective and novel spatial transcriptomics research.

RESULTS

VR-Omics enables end-to-end ST analyses in 2D and 3D

With VR-Omics, we developed the first automated interactive tool with a graphical user interface (GUI) that allows both the concatenation and analysis of multiple co-planar slices, as well as the generation of a harmonised coordinate system of stacked multi-slice tissues. This integration is achieved through the utilisation of the Unity Gaming Engine combined with Python-based analysis workflows (**Supplementary Methods**).

For the analysis of multiple co-planar slides, we have engineered a user interface utilising the Unity engine (**Fig. 1a**). This interface enables users to visualise and manipulate tissue slides, allowing them to be freely arranged and rotated to approximate the original structure of the tissue. This spatial arrangement is captured in the *world space* of Unity, where the relative positions of the tissue slides are meticulously collected. These coordinates are subsequently transferred to a Python-based workflow, which concatenates the data objects according to their spatial alignment. Rotation of the slices is facilitated by applying transformation matrices to the array of data points. Once aligned, the separate data objects are concatenated into a single entity and converted into required formats typically compatible with downstream processes. Additionally, the interface provides options for users to input filtering and processing parameters necessary for subsequent analysis.

In a parallel development for native 3D structures, VR-Omics includes a similar Unity-based user interface that supports the rotation and alignment of consecutive sections (**Fig. 1b**). This functionality allows for the visualisation of these sections as a cohesive 3D dataset, providing a comprehensive view of the tissue's architecture.

These automated workflows, enhanced with a user-friendly interface, not only streamline the analysis of multi-sliced tissue sections but also minimise inconsistent analytical steps or parameters across slices. This is achieved by standardising the analysis process across various open-source programming languages, promoting consistency, and reducing variability that arises when using multiple packages and coding languages.

To demonstrate the comprehensive capabilities of VR-Omics, we conducted an extensive evaluation on common analysis workflows encompassing data input/export handling, visualisation, and general utility, among a broad spectrum of ST tools outlined in **Fig. 1c** [6, 7, 10, 13, 17-21]. We systematically identified the essential steps required for analysing both co-planar multi-sliced tissues and depth-stacked datasets. Our comparison with a diverse array of SRT tools revealed that VR-Omics is the only platform capable of executing all necessary procedures integral to this analysis (**Fig. 1c**). This underscores the necessity of a unified platform that consolidates comprehensive data analysis within a single environment, as these tasks often require integrating multiple tools and navigating diverse coding languages such as R and Python.

3D reconstruction workflow of the developing human heart

To illustrate the capabilities of VR-Omics in comparison against multi-slice ST tools, we performed an in-depth analysis of a 3D multi-sliced dataset derived from the developing human heart using publicly available data (**Fig 2, Supplementary Table 1**). Our comparative

analysis employed a five-step workflow designed to cover all the necessary procedures for standard differentially expressed gene (DEG) analysis, applied specifically to spatial gene expression in different chambers of the developing human heart using a published 3D SRT dataset at 6 days post-conception (dpc) [22]. The workflow included: (1) inputting SRT data; (2) clustering spots/locations; (3) assembling slices into a 3D structure; (4) manually selecting two regions of interest (ROIs); and (5) identifying the top DEGs between these ROIs (**Fig. 2a**). This approach is critical for unraveling spatial gene expression patterns and comprehending the architectural complexities of tissues, where preserving the native 3D context is crucial for understanding the developmental intricacies that shape complex organ structures such as the heart.

We conducted this workflow comparing VR-Omics against several other tools: STitch3D [23], VR-Cardiomics [12], Loupe Browser [19], Xenium Desktop-Explorer [18], MERSCOPE Web-Vizualizer [20], Stereopy [17], SODBView (through its visualiser SOView) [10] and VT3D [7] (**Fig. 2, Supplementary Figure 1, Supplementary Table 1, Supplementary Methods**). Each tool was evaluated based on its ability to complete each workflow step, with scores assigned for full (score=1), partial (score=0.5), or unsuccessful (score=0) execution.

Firstly, the comparative analysis underscored that most tools are tailored primarily for 2D data, with limited capabilities for integrating 2D slices into a coherent 3D structure. Accordingly, all tools compared except VR-Omics, VR-Cardiomics, Stitch3D and VT3D were not able to proceed beyond completing task 3. Secondly, while VT3D and STitch3D support the assembly of 2D slices into 3D, they lack functionality for native 3D ROI selection, limiting the ability to isolate and investigate spatially restricted cell populations across the 3D stack. Thirdly, our previous tool, VR-Cardiomics, facilitates steps 3 to 5 of the workflow but is constrained by its

114 inability to process novel input data, highlighting VR-Omics' unique flexibility and
115 comprehensive support for 3D SRT data analysis [12]. Notably, only VR-Omics achieved a
116 perfect score across all five steps, showcasing its unparalleled capacity for conducting
117 comprehensive 3D spatial analyses and DEG identification (**Supplementary Tables 1-2**).

118

119 Understanding molecular signatures of paediatric cardiac rhabdomyomas using 120 VR-Omics

121 To further illustrate VR-Omics' unique end-to-end capabilities in the analysis of multi-slice
122 datasets, we tested it on an original co-planar dataset to interrogate a disease mechanism that
123 has not previously been transcriptomically investigated. Cardiac rhabdomyomas (cRMs) are
124 non-cancerous tumours that, while extremely rare in the general population, with a prevalence
125 between 0.0017%-0.28%, are the most common form of primary cardiac paediatric tumour [16,
126 24]. Depending on the anatomical presentation of cRMs in cardiac muscle these tumours can
127 impair normal heart function in a paediatric cohort by causing respiratory distress, arrythmias,
128 ventricular obstructions and cardiac failure [25, 26]. When their presence leads to severe health
129 complications, treatment options are very limited and include surgical resection [25], which
130 may lead to additional mortality and morbidity complications for the patient [24]. Yet, the
131 molecular mechanisms underlaying cRM formation remain unknown. Limited transcriptomics
132 studies of 10 marker genes have been performed on these tumours, identifying abnormal
133 regulation of the mTOR signalling pathway associated with cell proliferation [27]. To elucidate
134 the molecular and cellular perturbations leading to these abnormal cell populations and to

135 explore tumour heterogeneity in a spatial context, we profiled multiple cRMs with 10X
136 Genomics Visium platforms and VR-Omics.

137 Samples were obtained from cRMs located in the ventricles of two separate patients. The first
138 sections, MCHTB302, were obtained from a patient diagnosed with Birt-Hogg-Dubé Syndrome
139 (BHDS) who had two cRMs, one in the left ventricular cavity and a second in the apex of the
140 heart (**Fig. 3a**$_{i}$). For this study, two sections were taken from the cRM located in the left
141 ventricular cavity (**Fig. 3a**$_{ii\text{-}iii}$). Initial immunofluorescence staining performed on this tumour
142 indicated evidence of proliferating cardiomyocytes through colocalized staining of cTNT and
143 Ki-67 (**Fig. 3a**$_{iv}$) [28]. The section originating from the center of the tumour was then divided
144 across 3 Visium slides, due to size limitations of the Visium capture area (**Fig 3b-c**). The 3 slides
145 were easily and quickly recombined using VR-Omics to generate a single data object from the
146 multi-slice, co-planar dataset that more faithfully recapitulated the biological sample (**Fig. 3b-**
147 **c**). Using the STAGATE algorithm which was specifically developed for SRT clustering and is
148 implemented in VR-Omics' AW, we identified cell populations (cluster 0 and 4) in this dataset
149 that displayed a switch in cellular metabolism to increased aerobic respiration and oxidative
150 phosphorylation when their markers (*ACO2, ATP5F1A, ATP5F1B, ATP5ME, COX4I1*) were used
151 as an input for a gene ontology enrichment analysis (**Fig. 3d**). These populations may generate
152 additional ATP through upregulation of genes such as *ATP5IFI*, paralleling aspects of the
153 Warburg effect which sustains abnormal cell proliferation in cancerous tumours [29]. These
154 populations may generate additional ATP through upregulation of genes such as *ATP5IFI*,
155 paralleling aspects of the Warburg effect which sustains abnormal cell proliferation in
156 cancerous tumours [29]. These findings are in line with metabolic changes observed in murine
157 models with mutated or knocked out *FLCN*, similar to the patient's genotype, that are
158 proposed to be due to the dysregulation of the AMPK-mTOR pathway [30, 31]. *FLCN* has

159 previously been suggested to play a role in cardiac homeostasis and this lack of regulated
160 cellular energy levels may be driving this abnormal proliferation of cardiomyocytes [30]. *FLCN*
161 is implicated in other cardiac diseases such as cardiac hypertrophy, and therefore may be one
162 of many dysregulated genes giving rise to cRMs [30].

163 We then sought to validate this upregulation of oxidative phosphorylation and aerobic
164 respiration in the clusters identified through the STAGATE algorithm. First, we validated the
165 signature against an additional tumour section taken from the same patient, that did not need
166 to be divided across Visium capture areas (**Fig. 3e**). This served to confirm that the molecular
167 signatures were not an artefact from VR-Omics' multi-slice, co-planar analytical approach.
168 Using the same analytical pipeline this additional sample from MCHTB302 displayed the same
169 signature for up-regulation of pathways related to aerobic respiration in clusters located in the
170 centre of the tumour (**Fig. 3f**). Therefore, we demonstrate that VR-Omics' provides a unique
171 capacity for analysing co-planar datasets to explore novel biological mechanisms in rare tissue
172 sections.

173 We were fortunate to have access to samples from a second patient to investigate the presence
174 of the transcriptional signature across cRMs with distinct etiologies. The second patient
175 MCHTB361 presented with a cRM in the left ventricular outflow tract and had been diagnosed
176 with Tuberous Sclerosis Complex (TSC) which is commonly linked to cRMs [27] (**Fig 4a**). Three
177 separate sections were taken from this cRM, and each was captured using individual Visium
178 slides (**Fig. 4a**). Across all three sections, the same signatures of upregulation of aerobic
179 respiration and oxidative phosphorylation were present in clusters in the centre of the tumour
180 (**Fig. 4b$_{ii}$ -c, Supplementary Fig. 9**). Within these predominantly abnormal cardiomyocyte
181 clusters (**Fig. 3 & Fig. 4**), there was evidence for altered transcriptional signatures through

182 increased expression of genes such as *SLC25A4* which is consistent with increased metabolic
183 activity [31]. Certain cell clusters also displayed upregulation of genes involved in the increase
184 of glycolysis, potentially indicating the presence of the Warburg effect which may contribute
185 to the growth of these benign tumours [29]. Moreover, the clustering performed across
186 samples reveals additional transcriptional heterogeneity that cannot be identified using
187 histological analysis of single-slice data sets (**Fig. 2 & Fig. 3**).

188 These two avenues for validation demonstrate that the molecular signatures we identified are
189 robust in both intra- and inter- patient samples. The ability to generate a single data object
190 across multiple planar Visium sections allowed for a better understanding of the distribution
191 of cell populations across the tumour, which would have otherwise been lost due to artificial
192 tissue separation across capture areas. VR-Omics GUI makes this process easy and intuitive by
193 simplifying data joining to a simple 'drag and drop' alignment exercise of Visium slices within
194 the VR-Omic's GUI, eliminating the need for computational steps to generate a single data
195 object (**Supplementary Video 1**).

196 Subsequently we expanded our analysis to samples from a third patient (MCTHB362) who
197 presented with two cRMs, in the left atrium and atrial valve, and whose father was a known
198 carrier of TSC (**Fig. 4c**). The goal was to investigate further similarities between patients and
199 identify potential differences that may arise due to atrial and ventricular signatures between
200 the cRMs. For MCHTB362, tissue from both cRMs had to be sectioned to accommodate Visium
201 size restrictions and were later virtually reconstructed like the samples from MCHTB302 (**Fig.
202 4c & Supplementary Fig. 8e**). This allowed direct comparison of multi-slice, co-planar
203 datasets between patients to determine if similar signatures were present. Moreover, the
204 presence of a single section that fit on an individual Visium slide (**Fig. 4c**) allows for intra-

205 sample comparison for merged or individual data objects. In this instance, we noticed that the
206 cRMs originating in the atria had a slightly different transcriptional profile than previous
207 ventricular samples (**Fig. 3 & Fig. 4d**). However, upregulation of aerobic metabolism in certain
208 clusters remained constant, demonstrating a consistent association with the tumour
209 phenotype across all patients (**Fig. 3 & Fig. 4d**). Processing and visualization of multiple
210 patient samples through VR-Omics facilitated the discovery of similar cell populations and
211 molecular signatures in MCTHB302 and MCHTB361 that suggest they are characteristic of
212 cRMs (**Fig 3-5 and Supplementary Fig. 9**). This signature was also present within MCHTB362
213 despite these samples being histologically and transcriptionally distinct from MCHTB302 and
214 MCHTB361 (**Fig. 3-5 and Supplementary Fig. 9**). These findings across patients were further
215 orthogonally validated outside of the VR-Omics framework (**Supplementary Results**).
216 Altogether this provides evidence that this switch to an altered transcriptional signature to
217 increase aerobic respiration is characteristic of the cRMs in all three patients (**Fig 3-5 and**
218 **Supplementary Fig 9**).

219 DISCUSSION

220 The number of multi-slice ST experiments is growing rapidly [32], simultaneously presenting a
221 great opportunity for spatial biology investigations and a data science challenge. Addressing
222 To address the gap in technologies capable of handling multi-slice data, VR-Omics was
223 designed from the ground up to manage multi-slice ST data (both co-planar and 3D stacked)
224 through an intuitive, customizable graphical interface that requires minimal computational
225 skills (**Supplementary Fig. 2, Supplementary Video 1**). When compared to multiple tools
226 and pipelines for SRT data analysis, VR-Omics demonstrates its unique capability in performing
227 comprehensive and advanced end-to-end data analysis for multi-slice SRT datasets.

228 Benchmarking VR-Omics against most common SRT data analysis and visualisation tools using
229 the 3D human developing heart dataset reveals that only VR-Omics fulfils all the necessary
230 criteria for end-to-end analysis and visualisation typically of interest to biologists in a 3D
231 stacked dataset.

232 The space of SRT data analysis urgently requires applications developed for 3D datasets to
233 align, visualise and process multi-sliced data. At the time of writing, only STich3D [6], VT3D [7]
234 and our previous work VR-Cardiomics [12] support 3D data visualisation and analyses besides
235 VR-Omics. However, these applications focus on delivering specific aspects of the analytical
236 pipeline, and therefore lack critical features to enable end-to-end analysis for users with a
237 range of computational expertise. For example, VR-Cardiomics lacking the ability to analyse
238 users' novel data, rather focusing on visualisation of a singular pre-processed dataset. Which
239 removes the flexibility of extending the tool to new studies. Thus, we have developed VR-
240 Omics to bridge this gap, allowing users to analyse and interact with their 3D data in an
241 intuitive manner.

242 Our comparative analysis between VR-Omics and other proprietary and open-source tools for
243 ST multi-slice analysis (**Fig. 1c**), reflects a wide range of support for various SRT platforms and
244 the advanced analytical tasks required by researchers. Despite the inclusion of tools specialised
245 for enhancing spatial analysis in three dimensions, such as Stitch3D and VT3D, which primarily
246 focus on visualization and data mining, only VR-Omics was able to complete all five essential
247 steps for a comprehensive analysis (**Fig 2, Supplementary Table 1**). This evaluation confirmed
248 VR-Omics' unique ability to support a complete analytical workflow, significantly
249 outperforming existing methodologies in efficiency and thoroughness of data analysis. VR-
250 Omics' singular success in completing all steps of the biological case study, particularly in

251 identifying differentially expressed genes between two cardiac regions, further highlights its
252 unparalleled capability to provide a robust and comprehensive framework for analysing
253 complex spatial transcriptomics data.

254 Through the analysis of rare cRM samples we demonstrate that VR-Omics overcomes two
255 major challenges in multi-slice co-planar ST data: (1) biologically adjacent samples being
256 separated for processing which need to be merged for analysis, and (2) inter-sample
257 comparisons. VR-Omics' capability to analyse multi-slice datasets and easily perform inter-
258 sample comparisons permitted the elucidation of key molecular mechanisms contributing to
259 the growth of rare cardiac rhabdomyoma samples. The workflow available within the VR-Omics
260 framework identified shared signatures of increased aerobic respiration across patients within
261 abnormal cardiomyocytes faster than comparable workflows implemented across multiple
262 disaggregated packages. This indication of potential dysregulation of the AMPK-mTOR
263 pathway is known to have an effect on mitochondrial metabolism and has been demonstrated
264 in murine models with mutations in *FLCN*, the same gene known to be mutated in patient
265 MCHTB302 [30]. Without effective analysis of SRT data through framework tools such as VR-
266 Omics, rare clinical samples preserved in FFPE such as these cRMs (prevalence 0.0017%-0.28%),
267 would remain inaccessible.

268 CONCLUSION

269 Multi-slice ST data analysis is quickly evolving [33], and VR-Omics rapidly evolves to address
270 development and improvement cycles. VR-Omics natively supports multi-slice ST data from
271 Visium, Xenium, Stereo-Seq and MERFISH, and will support Nanostring (CosMX) and Slide-Seq
272 V2 in the near future. By addressing existing computational limitations in current multi-slice
273 ST tools, VR-Omics offers unique advantages as demonstrated in this study using both stacked

and co-planar multi-slice datasets. In this study we leverage VR-Omics to dissect the mechanisms underlying growth of paediatric cRMs. Our discovery unlocks potential insights into the regeneration of cardiac muscle for therapeutic purposes as the tumours develop within striated muscle and cause abnormal levels of proliferation after birth. VR-Omics stands out from other tools with unique software architecture, immersive environment, cross-platform compatibility, and a fully automated workflow, all aiming at simplifying and democratising ST analyses in the spatial biology community.

MATERIAL AND METHODS

VR-Omics Architecture

To deliver a seamless user experience, VR-Omics was conceived as a sophisticated end-to-end analysis tool, integrating two primary components via a user-friendly interface (**Supplementary Fig. 3**). The first component, the purpose-built Automated Workflow, focuses on the processing and mining of raw SRT data (**Supplementary Fig 3a, b**). The second component, the Visualiser, utilises the processed data to facilitate advanced data visualization, equipped with multiple features for enhanced data interaction and exploration through a fully interactive interface, designed with intuitive data mining processes in mind (**Supplementary Fig 3c, d**).

VR-Omics was developed utilising the Unity game development engine by Unity Technologies, starting with Unity version 2019.4.26f1. An upgrade to version 2021.3.11f1 (Long-Term Support, or LTS) was later implemented to ensure complete compatibility with the Virtual Reality toolkit plugin (XR Interaction Toolkit version 2.0.3) (**Supplementary Methods**). For each integrated SRT platform, we developed specific state-of-the-art Automated Workflows

using Python executables and open-sourced tools and packages, which are embedded within the application to function as a unified software solution.

Features of VR-Omics

Automated Workflow

For each of the integrated SRT platforms, a purpose-built Automated Workflow (AW) was developed to optimize data processing and allow advanced analysis of the SRT raw data. This optimization is achieved through a user-friendly interface that enables end-to-end processing and analysis of raw data, thus eliminating the need for time-consuming data formatting steps. All proprietary data is supported as provided by the vendor, and VR-Omics automatically detects the necessary files by selecting the main directory of each sample, reducing the risk of incorrect file selection. Within the AW, users can perform a variety of operations to tailor data analysis (**Supplementary Fig. 2a-d**), including standard filtering metrics to ensure data quality such as: (i) number of counts per location, (ii) percentage of overall mitochondrial gene expression, and (iii) number of cells expressing a certain gene. These metrics can all be easily visualised across the tissue section to highlight regions of poor data quality and capture inter- or intra-tissue heterogeneity (**Supplementary Fig. 2a**).

The default normalisation methods (as recommended by each analysis package) are applied, and data is log-transformed before highly variable genes (HVGs) are identified. Subsequently, principal component analysis (PCA) is performed, neighbours are computed, and UMAP or t-SNE coordinates are generated prior to performing spatially agnostic Leiden clustering or STAGATE-enhanced Leiden clustering depending on the dataset (**Supplementary Fig. 2b**). The AW executes spatial analyses using various Python libraries such as Scanpy, SpatialDE,

318 STAGATE, and SpaceFlow, among others, for different commercialised and open-source SRT
319 platforms and custom data (**Supplementary Fig. 3b**).

320 Spatially variable genes (SVGs), crucial for understanding cell differentiation and tissue
321 organisation, are identified using SpatialDE for Visium data or Moran's I statistic for other data
322 types (**Supplementary Fig. 2c**) [34]. These steps, selected to follow a typical workflow of a
323 bioinformatician, ensure VR-Omics provides a complete experience for the analysis. Additional
324 capabilities for Visium datasets include the option to concatenate multiple sections from the
325 same tissue in 2D for downstream joint analysis (**Supplementary Fig. 2e**) and the exploration
326 of clustering results using the Leiden algorithm or STAGATE for more complex analyses.

327 Visualiser Capabilities

328 Across these SRT platforms, different terms are used for the smallest individual capture area
329 of each technique, *e.g.*, *spots*, *locus/loci*, *bins,* or *locations*. For consistency we will henceforth
330 use the term *locations*, always referring to the smallest individual capture area of the respective
331 SRT methods.

332 After processing their data through the Automated Workflow (AW) or loading the requisite
333 files, irrespective of the data platform used, users can explore their datasets within the
334 Visualiser. The Visualiser offers an array of interactive features designed with input from
335 biologists to create intuitive analysis tools and ensure availability of the right resources to
336 address various biological questions. These features support the systematic exploration and
337 comparison of gene expression data across samples within a 2D desktop or VR environment
338 (**Supplementary Fig. 4-5, Supplementary Table 3**).

339 Key capabilities include the visualisation of gene expression, enabling insights into the
340 expression of significant markers, such as EPCAM in breast cancer, which is associated with
341 poor prognosis [35]. This visualization aids in correlating disease severity with tissue
342 characteristics, further enhanced by the superimposition of metadata like clustering results or
343 images alongside gene expression data, allowing for rapid assessment of alignment between
344 clustering, gene expression, and tissue histology.

345 The platform also enables the exploration of gene expression profiles, crucial for leveraging
346 the full potential of SRT data. Features like visualising two different gene expression profiles
347 on adjacent slides or within the same tissue section, as well as vector-based gene expression
348 differences, facilitate comparisons of markers linked to disease prognosis or aggressiveness
349 such as *EPCAM* and *ELF3* in breast cancer [35, 36]. This comparison is valuable for
350 understanding their impact on specific regions or cells within a tumour. Replication of actions
351 across duplicated slides, such as region of interest (ROI) selection, is supported.

352 Gene search functionality allows users to find and visualise a gene of interest's expression
353 through a heatmap, showcasing relative expression at each location (**Supplementary Fig. 4a**).
354 An alternative binary visualisation mode highlights locations with nonzero expression of the
355 selected gene, enhancing the visibility of gene activity (**Supplementary Fig. 4a**). Users can
356 adjust the visualization granularity by modifying location size or filtering out low-expression
357 locations, applying thresholds to streamline the display (**Supplementary Fig. 6e**). If SVGs were
358 identified using the AW, these genes are highlighted with a turquoise-coloured result button
359 for easy identification (**Supplementary Fig. 6b**).

Superimposition of other metadata, such as H&E staining or clustering results from Leiden or spatial clusters calculated in the AW, is facilitated for enhanced data interpretation (**Supplementary Fig. 6d**). When available, serial sections across a sample enable the uploading of a 3D model to improve spatial and anatomical orientation (**Supplementary Fig. 4c**), with various adjustments available to align the 3D model with the dataset.

The Visualiser's side-by-side comparison feature allows visualization of two different gene expression profiles on adjacent slides or the same tissue section, enabling precise ROI delineation and ensuring identical analysis areas across slides. This feature can be toggled off to merge the expressions of both genes into a normalised, vector-based difference calculation at each location, highlighting significant expression differences between the two gene profiles (**Supplementary Fig. 4e-f**).

Facilitating analysis of multi-slice Visium Datasets

For Visium datasets, VR-Omics overcomes two common analytical challenges: (1) facilitating concatenation of multiple Visium sections taken from the same tissue in 2D for joint analysis (**Supplementary Fig. 2e**) and (2) loading of multiple, serial sections for visualisation in 3D (**Supplementary Fig. 2f**). The first feature is enhanced through the introduction of a visually intuitive concatenation interface. Here, each sample is represented by its histologically stained image, allowing users to rearrange slides into their original configuration via a user-friendly drag-and-drop mechanism. Additionally, slides can be effortlessly rotated, enabling precise and flexible alignment for the accurate reconstruction of original tissue sections. Following alignment, users have the capability to specify processing parameters, including the filtering of cells, genes, and mitochondrial values, as well as adjusting the sensitivity of the clustering

algorithm. These inputs initiate the seamless concatenation of slides, followed by subsequent analyses and cell type clustering, streamlining the entire process for optimal data integration and interpretation.

In the second scenario, VR-Omics offers the unique option to simultaneously load multiple Visium samples if they represent serial sections of the same tissue, to visualise the tissue in 3D (**Supplementary Fig. 2f**). For this, VR-Omics provides a straightforward alignment process consisting of selecting multiple Visium sample folders that have been processed and/or analysed with the AW (**Supplementary Fig. 2f$_{i}$**). The selected datasets will be in unison, allowing the user to set the correct anatomical order from front to back of the slides. Next, all Haematoxylin and Eosin (H&E) images will be overlapped in a simple user interface that allows the user to rotate the slides individually, correcting misalignments of the samples on the capture areas (**Supplementary Fig. 2f$_{ii}$**). Furthermore, the user can set the distances between each slide in depth direction (**Supplementary Fig. 2f$_{ii}$**). Finally, the user can visualise the merged dataset rendered from the selected slides with the set distances and rotations as a 3D object (**Supplementary Fig. 2f$_{iii}$**).

The virtual reconstruction offered through VR-Omics GUI allows datasets to be interpreted by biologists in a representation that is more faithful to the whole tissue. To provide training for prospective users, the AW and Visualiser capabilities can be explored by processing of the 3D demo data of the human developing heart [22]. When dealing with 3D datasets, the user can upload a 3D model of their tissue or organ of interest and align spatial data within it. In the case of the developing human heart [22], an overlay of the 3D model provides the user a more intuitive understanding of which clusters correspond to anatomical structures within the heart,

allowing for easier selection of biologically relevant regions of interest (ROIs) across the depth of the dataset (Supplementary Fig. 4d).

Processing patient samples and data analyses

Human ethics for cardiac tissue biobanking and human pluripotent stem cell research was approved by The Royal Children's Hospital Melbourne Human Research Ethics Committee (approval numbers: HREC 38192). Informed consent was obtained from all human participants, and studies were conducted in accordance with the approved protocols and guidelines from the National Health and Medical Research Council of Australia. All samples were sequenced using the Visium FFPE Spatial Solution in conjunction with the Advanced Genomics Facility at the Walter and Eliza Hall Institute (WEHI). Samples of patient MCTHB302 were sequenced in the first batch, while the samples of MCTHB361 and of MCTHB362 were sequenced in a subsequent batch. Samples were sectioned as necessary to fit Visium capture areas (**Fig. 3,5 and Supplementary Fig. 8).** Outputs from both batches of Visium experiments were reanalysed through the SpaceRanger pipeline v2.0.1 [37] by the WEHI team. The outputs of the SpaceRanger pipeline for all samples were used as the inputs VR-Omics. This included using the Visualiser to align multiple 2D slices and generated a joint, co-planar data object (**Supplementary Video 1**), and Scanpy pre-processing including clustering using STAGATE. Filter parameters were established independently for each sample. Then markers for each cluster were used as the input for gene ontology enrichment analysis using Metascape [38] or Webgestalt [39].

These findings were then validated orthogonally, outside of the VR-Omics framework using a series of comparable tools requiring coding experience. Samples were pre-processed and filtered in Seurat then clustering for individual or joint objects for all patients was performed

using the BayesSpace algorithm [40]. Gene ontology enrichment analysis was performed as outlined above.

Availability of data and materials

The project home page providing VR-Omics software, tutorial, and demos is available under https://ramialison-lab.github.io/pages/vromics.html.

VR-Omics can also be accessed directly via https://figshare.com/articles/software/VR-Omics_Exploration_of_Spatial_Transcriptomics_data_in_3D/24503611. The source code can be accessed via https://github.com/Ramialison-Lab/VR-Omics

The paediatric cardiac rhabdomyomas patient Visium profiling data are available on NCBI GEO with accession number GSE252228. Third-party datasets used in this study: EGAS00001003996 [22]. Data for cross-platform comparison are available at https://figshare.com/s/78bcc6320cf3b2ee64af.

Custom R scripts for visualising Stitch3D data are available at https://figshare.com/s/0c9d9cc265b45b5d9441.

Supplementary Information

Supplementary Results

Additional results for cross-platform comparisons of mouse brain slides across multiple ST platforms are available. More information on multi-slice 3D data analysis using VR-Omics and orthogonal validation of up-regulated pathways in cRMs is also provided.

Supplementary Methods

Additional information about the input data for ST platforms, the technical specifications of VR-Omics and its corresponding AW implementation, and the features of VR-Omics is

provided. Furthermore, there is additional information on the analysis of cRMs using BayesSpace.

Supplementary Table 1: Benchmarking use case comparison and scoring between VR-Omics, STich3D, VR-Cardiomics, Loupe Browser, Xenium Desktop Browser, MERSCOPE Web-Vizualizer, Stereopy and SODB.

Supplementary Table 2: List of differentially expressed genes between the right ventricle and right atrium identified in the human embryonic heart at 6 dpc by VR-Omics.

Supplementary Table 3: Overview of all features supported by VR-Omics indicating for which SRT method they are available.

Supplementary Table 4: Feature comparison of VR-Omics with commonly used visualisation tools for each of the SRT methods supported by VR-Omics. The features described in this table show the overall capability of VR-Omics compared to the tools that are available to visualise and explore SRT data.

Supplementary Video : Overview of capabilities of VR-Omics.

AUTHOR CONTRIBUTIONS

Conception and design: DB, NC, ERP, DAE, KK, HTN, FS, MR. Data acquisition, analysis and interpretation: DB, NC, HC-S, DM, BC, ATP, ERP, DAE, HTN, MR. Software development: DB, NC, DW, SJ-H, DG, JS, HTN. Manuscript draft: DB, NC. Manuscript editing and review: all authors.

ACKNOWLEDGEMENTS

We thank the patient donors and their family for the valuable samples. We thank the members of the Ramialison's, Schreiber's, Porrello's, and Elliott's lab, especially Antonia Zech, Sebastian Bass-Stringer and Grzegorz Maciag for helpful discussions. We thank Celine Vivien for early staining and imaging of cRM samples that later informed experimental design. We thank the support of the WEHI Advanced Genomics Facility for technical advice on processing the patient samples. We thank Brett Kennedy and Patrick Marks (10x Genomics) and Jan Philipp Junker and Jeroen Bakkers for the sample data. We thank Yuen Chang and Jacquie Crawford and Francesca Bolk for support and assistance. We thank Geoff McDermott and Catherine King from 10x Genomics for their support and advice with the Visium platform. We thank Lisa Waylen and Maria Nucera for their helpful feedback on manuscript drafts.

FUNDING

MR and HTN are supported by an NHMRC Ideas Grant (APP1180905). MR is funded by a Heart Foundation Future Leader Fellowship. NC is supported a 10x-Millenium Science's Spatial Pioneer fellowship. Additional infrastructure funding to the Murdoch Children's Research Institute was provided by the Australian Government National Health and Medical Research Council Independent Research Institute Infrastructure Support Scheme. The Australian Regenerative Medicine Institute is supported by grants from the State Government of Victoria and the Australian Government. The Novo Nordisk Foundation Center for Stem Cell Medicine is supported by Novo Nordisk Foundation grants (NNF21CC0073729).

CONFLICT OF INTEREST

ERP is a cofounder, scientific advisors, and holds equity in Dynomics, a biotechnology company focused on the development of heart failure therapeutics. NC was an employee of Dynomics.

492 # REFERENCES

493 1. Marx, V. and (2021) Method of the Year: spatially resolved transcriptomics. ***Nature***
494 ***Methods***, 18, 9-14.
495 2. Cheng, M., Jiang, Y., Xu, J., Mentis, A.A., Wang, S., Zheng, H., Sahu, S.K., Liu, L. and Xu,
496 X. (2023) Spatially resolved transcriptomics: a comprehensive review of their
497 technological advances, applications, and challenges. ***J Genet Genomics***, 50, 625-640.
498 3. Zeira, R., Land, M., Strzalkowski, A. and Raphael, B.J. (2022) Alignment and integration
499 of spatial transcriptomics data. ***Nature Methods***, 19, 567-575.
500 4. Berglund, E., Maaskola, J., Schultz, N., Friedrich, S., Marklund, M., Bergenstråhle, J.,
501 Tarish, F., Tanoglidi, A., Vickovic, S., Larsson, L. *et al*. (2018) Spatial maps of prostate
502 cancer transcriptomes reveal an unexplored landscape of heterogeneity. ***Nature***
503 ***Communications***, 9, 2419.
504 5. Chen, A., Liao, S., Cheng, M., Ma, K., Wu, L., Lai, Y., Qiu, X., Yang, J., Xu, J., Hao, S. *et al*.
505 (2022) Spatiotemporal transcriptomic atlas of mouse organogenesis using DNA
506 nanoball-patterned arrays. ***Cell***, 185, 1777-1792.e1721.
507 6. Wang, G., Zhao, J., Yan, Y., Wang, Y., Wu, A.R. and Yang, C. (2023) Construction of a 3D
508 whole organism spatial atlas by joint modelling of multiple slices with deep neural
509 networks. ***Nat Mach Intell***, 5, 1200–1213.
510 7. Guo, L., Li, Y., Qi, Y., Huang, Z., Han, K., Liu, X., Liu, X., Xu, M. and Fan, G. (2023) VT3D: a
511 visualization toolbox for 3D transcriptomic data. ***J Genet Genomics***, 50, 713-719.
512 8. Fan, Z., Chen, R., Chen, X. and (2020) SpatialDB: a database for spatially resolved
513 transcriptomes. ***Nucleic Acids Research***, 48, D233-D237.
514 9. Xu, Z., Wang, W., Yang, T., Chen, J., Huang, Y., *et al*. (2024) STOmicsDB: a database of
515 Spatial Transcriptomic data. ***Nucleic Acids Research***, 52(D1):D1053-D1061.
516 10. Yuan, Z., Pan, W., Zhao, X., Zhao, F., Xu, Z., *et al*. (2023) SODB facilitates comprehensive
517 exploration of spatial omics data. ***Nature Methods***, 20(3):387-399.
518 11. Li, Y., Dennis, S., Hutch, M.R., Li, Y., Broad, M.S., *et al*. (2022) SOAR: a spatial
519 transcriptomics analysis resource to model spatial variability and cell type interactions.
520 ***BioRXiv*** 2022.04.17.488596.

12. Bienroth, D., Nim, H.T., Garkov, D., Klein, K., Jaeger-Honz, S., *et al*. (2022) Spatially resolved transcriptomics in immersive environments. ***Vis Comput Ind Biomed Art***, 5(1):2.
13. Ma, S., Fang, X., Yao, Y., Li, J., Morgan, D.C., Xia, Y., Kwok, C.S.M., Lo, M.C.K., Siu, D.M.D., Tsia, K.K. *et al*. (2023) StarmapVis: An interactive and narrative visualisation tool for single-cell and spatial data. ***Comput Struct Biotechnol*** J, 21, 1598-1605.
14. Yang, A., Yao, Y., Fang, X., Li, J., Xia, Y., *et al*. starmapVR: immersive visualisation of single cell spatial omic data. ***bioRxiv***, 2020.09.01.277079.
15. Bondavalli, D., White, S.M., Steer, A., Pflaumer, A., Winship, I. and (2015) Is cardiac rhabdomyoma a feature of Birt Hogg Dubé syndrome? ***Am J Med Genet A***, 167A, 802-804.
16. Holley, D.G., Martin, G.R., Brenner, J.I., Fyfe, D.A., Huhta, J.C., *et al*. (1995) Diagnosis and management of fetal cardiac tumors: a multicenter experience and review of published reports. ***J Am Coll Cardiol***, 26, 516-520.
17. Stereopy. URL: https://stereopy.readthedocs.io/en/latest/index.html
18. Xenium Explorer - 10x Genomics. URL: https://www.10xgenomics.com/support/software/xenium-explorer/latest
19. Loupe Browser - 10x Genomics. URL: https://www.10xgenomics.com/support/software/loupe-browser/latest
20. MERSCOPE Spatial Transcriptomics - Vizgen. URL: https://vizgen.com/vizgen-merscope/
21. Sztanka-Toth, T.R., Jens, M., Karaiskos, N. and Rajewsky, N. (2022) Spacemake: processing and analysis of large-scale spatial transcriptomics data. ***GigaScience***, 11, giac064.
22. Asp, M., Giacomello, S., Larsson, L., Nilsson, M., Lundeberg, J. and (2019) A Spatiotemporal Organ-Wide Gene Expression and Cell Atlas of the Developing Human Heart. ***Cell***, 179, 1647-1660.e1619.
23. Wang, G., Zhao, J., Yan, Y., Wang, Y., Wu, A.R., *et al*. (2023) Construction of a 3D whole organism spatial atlas by joint modeling of multiple slices. ***Nature Machine Intelligence***, 2023.2002.2002.526814.

24. Berger, J.T., Holubkov, R., Reeder, R., Wessel, D.L., Meert, K., Berg, R.A., Bell, M.J., Tamburro, R., Dean, J.M. and Pollack, M.M. (2017) Morbidity and mortality prediction in pediatric heart surgery: Physiological profiles and surgical complexity. ***J Thorac Cardiovasc Surg***, 154, 620-628.e626.
25. Joshi, M., Kumar, S., Noshirwani, A. and Harky, A. (2020) The Current Management of Cardiac Tumours: a Comprehensive Literature Review. ***Braz J Cardiovasc Surg***, 35, 770-780.
26. Irabor, B., Khan, A., Noga, M., Myers, K., Greenway, S.C. and Hassanabad, A.F. (2024) Arrhythmia as a Presenting Feature of Atypical Cardiac Rhabdomyoma in Children. ***CJC Pediatric and Congenital Heart Disease*** (in press).
27. Kotulska, K., Larysz-bRYSZ, M., Grajkowska, W., Jóźwiak, J., Włodarski, P., *et al*. (2011) Cardiac Rhabdomyomas in Tuberous Sclerosis Complex Show Apoptosis Regulation and mTOR Pathway Abnormalities. ***Pediatr Dev Pathol***, 12, 89-95.
28. Uxa S, Castillo-Binder P, Kohler R, Stangner K, Müller GA, Engeland K. (2021) Ki-67 gene expression. ***Cell Death & Differentiation***, 28:3357-3370.
29. Zhou B, Caudal A, Tang X, Chavez JD, McMillen TS, Keller A, Villet O, Zhao M, Liu Y, Ritterhoff J, et al. (2022) Upregulation of mitochondrial ATPase inhibitory factor 1 (ATPIF1) mediates increased glycolysis in mouse hearts. ***J Clin Invest***, 132.
30. Hasumi, Y., Baba, M., Hasumi, H., Huang, Y., Lang, M., *et al*. (2014) Folliculin (Flcn) inactivation leads to murine cardiac hypertrophy through mTORC1 deregulation. ***Human Molecular Genetics***, 23, 5706-5719.
31. King, M.S., Thompson, K., Hopton, S., He, L., Kunji, E.R.S., Taylor, R.W. and Ortiz-Gonzalez, X.R. (2018) Expanding the phenotype of de novo SLC25A4-linked mitochondrial disease to include mild myopathy. ***Neurol Genet***, 4, e256.
32. Lin, Y. and Yang, J.Y.H. (2022) 3D reconstruction of spatial expression. ***Nature Methods***, 19, 526-527.
33. Du, J., Yang, Y.C., An, Z.J., Zhang, M.H., Fu, X.H., *et al*. (2023) Advances in spatial transcriptomics and related data analysis strategies. ***J Transl Med***, 21(1):330 21, 330.
34. Svensson, V., Teichmann, S.A. and Stegle, O. (2018) SpatialDE: identification of spatially variable genes. ***Nature Methods***, 15, 343-346.

35. Soysal, S.D., Muenst, S., Barbie, T., Fleming, T., Gao, F., Spizzo, G., Oertli, D., Viehl, C.T., Obermann, E.C. and Gillanders, W.E. (2013) EpCAM expression varies significantly and is differentially associated with prognosis in the luminal B HER2(+), basal-like, and HER2 intrinsic subtypes of breast cancer. ***Br J Cancer***, 108, 1480-1487.
36. Zhang Z, Zhang J, Li J, Geng H, Zhou B, Zhang B, Chen H. (2020) miR-320/ELF3 axis inhibits the progression of breast cancer via the PI3K/AKT pathway. ***Oncol Lett***, 19:3239-3248.
37. Space Ranger - 10x Genomics. URL: https://www.10xgenomics.com/support/software/space-ranger/latest/getting-started/what-is-space-ranger
38. Zhou, Y., Zhou, B., Pache, L., Chang, M., Khodabakhshi, A.H., *et al.* (2019) Metascape provides a biologist-oriented resource for the analysis of systems-level datasets. ***Nat Commun*** 10, 1-10.
39. Liao, Y., Wang, J., Jaehnig, E.J., Shi, Z., Zhang, B. and (2019) WebGestalt 2019: gene set analysis toolkit with revamped UIs and APIs. ***Nucleic Acids Res*** 47, W199-W205.
40. Zhao, E., Stone, M.R., Ren, X., Guenthoer, J., Smythe, K.S., *et al.* (2021) Spatial transcriptomics at subspot resolution with BayesSpace. ***Nat Biotechnol*** 39, 1375-1384.
41. Human Breast Cancer (Block A Section 1) - 10x Genomics. URL: https://db.cngb.org/stomics/datasets/STDS0000027

TABLE AND FIGURES LEGENDS

Figure 1. Analytical capabilities of VR-Omics. **a**, Schematic overview of data generation and processing workflow for multi-slice co-planar ST datasets. **b**, Schematic overview of data generation and processing workflow for multi-slice 3D stacked ST datasets. **c**, Heatmap comparison of analytical features supported by VR-Omics and other available software for ST analysis. Software is outlined on the y-axis while analytical features are listed on the x-axis and coloured according to their applicability to multi-slice co-planar or 3D stacked datasets.

608 Features supported by the software are displayed in teal while unsupported features are
609 displayed in dark blue.

610 **Figure 2**. Cross-platform comparison for 3D reconstruction workflow of the developing human
611 heart. **a,** Schematic of workflow to identify differentially expressed genes between the right
612 atrium and right ventricle. **b**, Results from VR-Omics completing the workflow. On the left
613 the final visualisation of the right atrium (blue) and ventricle (red) are displayed within the
614 VR-Omics GUI and the spider plot on the right displays VR-Omics ability to complete all 5
615 steps of the workflow. **c**, Results from VT3D executing the workflow. On the left the final
616 visualisation of the right atrium and ventricle is displayed within VT3D and the spider plot on
617 the right displays its ability to complete 4/5 steps of the workflow. **d**, Results from VR-
618 Cardiomics executing the workflow using a mouse heart, with the chambers displayed on the
619 left and the spider plot on the right displaying the 3.5 steps that can be completed within
620 VR-Cardiomics. **e**, Example results from Stich3D executing the workflow with chambers
621 displayed and coloured on the left and the spider plot on the right. Selection of specific ROIs
622 to highlight the right atrium in black and right ventricle in red performed in R outside of the
623 STich3D framework. **g**, Spider plot demonstrating performance of remaining tools trailed for
624 this workflow.

625

626 **Figure 3.** Analysis of multi-slice co-planar and single slice ventricular MCHTB302 cardiac
627 rhabdomyoma data. $\mathbf{a_i}$, Schematic representing location of cRM used for data generation. $\mathbf{a_{ii}}$,
628 ECG displaying location of cRM in left ventricular cavity. $\mathbf{a_{iii}}$, Schematic representing
629 approximate locations of sections taken for data generation using the 10X Genomics Visium
630 platform. $\mathbf{a_{iv}}$**,** Immunostaining with Ki67 indicating proliferation within the tumour (orange); nuclei
631 staining (Hoescht, blue); cardiac troponin T (cTNT, green). **b,** Reconstruction and concatenation

632 within VR-Omics of 3 co-planar, H&E stained slices separated onto different Visium capture
633 areas due to size of the tissue. **c**, Example of STAGATE clusters visualised across the
634 reconstructed co-planar dataset (labelled as Sample 1 in panel a) within VR-Omics. **d**, Example
635 of STAGATE clusters visualised across the single section dataset (labelled as Sample 2 in panel
636 a) within VR-Omics. **e**, GO analysis results of multi-slice coplanar dataset using the STAGATE
637 cluster markers as inputs for Metascape. Oxidative phosphorylation and aerobic respiration
638 signatures are highlighted in a red box for clusters 1 and 5 located at the centre of the tumour.
639 **f**, GO analysis results of single-slice dataset using the STAGATE cluster markers as inputs for
640 Metascape. Oxidative phosphorylation and aerobic electron transport chain signatures are
641 highlighted in a red box for cluster 1 located at the centre of the tumour.

642 **Figure 4.** Analysis of single-slice MCHTB361 cardiac rhabdomyoma data. **a**, Schematic
643 representing location of cRM used for data generation. **b,** Analysis of a single slice MCHTB361
644 dataset within VR-Omics. **b_i**, H&E stained section visualised with VR-Omics**.** **b_{ii},** Example of
645 STAGATE clusters visualised dataset within VR-Omics. **c**, GO analysis results of single slice
646 dataset using the STAGATE cluster markers as inputs for Metascape. Oxidative
647 phosphorylation and aerobic respiration signatures are highlighted in a red box for clusters 1
648 and 5 located at the centre of the tumour. **f**, GO analysis results of single-slice dataset using
649 the STAGATE cluster markers as inputs for Metascape. Oxidative phosphorylation and aerobic
650 electron transport chain signatures are highlighted in a red box for clusters 1 and 3.

651 **Figure 5.** Analysis of multi-slice co-planar and single slice MCHTB362 atrial cardiac
652 rhabdomyoma data. **a**, Schematic representing location of cRMs used for data generation
653 using the 10X Genomics Visium platform. **b_i**, H&E stained single slice section visualised with
654 VR-Omics. **b_{ii}**, Example of STAGATE clusters visualised across a single-slice dataset within VR-

655 Omics. **c_i,** Reconstruction and concatenation within VR-Omics of 2 co-planar, H&E stained
656 slices separated onto different Visium capture areas due to size of the tissue. **c_{ii}**, Example of
657 STAGATE clusters visualised across the reconstructed co-planar dataset within VR-Omics. **d**,
658 GO analysis results of single dataset using the STAGATE cluster markers as inputs for
659 Metascape. Oxidative phosphorylation and aerobic electron transport chain signatures are
660 highlighted in a red box for clusters 2, 5 and 6 located at the centre of the tumour. **e**, GO
661 analysis results of multi-slice, co-planar dataset using the STAGATE cluster markers as inputs
662 for Metascape. Oxidative phosphorylation and cellular respiration signatures are highlighted
663 in a red box for clusters 2,3 and 6 located at the centre of the tumour.

664 **Supplementary Figure 1.** Top GO terms identified in Metascape when using the top
665 differentially expressed genes (DEGs) between the right atrium and right ventricle using VR-
666 Omics from the workflow to perform a 3D reconstruction of the human developing heart.

667 **Supplementary Figure 2.** Automated Workflow (AW). **a**, Data processing and filtering.
668 Accepted SRT data types for analysis, processing and filtering using the AW include Visium,
669 STOmics, MERFISH and Xenium. Analysis steps available to all SRT data types and menu with
670 examples of available visualisations after data analysis. On the right, an example of heatmap
671 of read counts generated for invasive ductal carcinoma breast tissue data generated with
672 Visium from 10X Genomics [41] . **b**, Leiden or STAGATE clustering analysis and visualisation of
673 clustering output using Visium data of the human cerebral cortex. **c**, Identification of SVGs is
674 performed using SpatialDE for Visium data and by calculating Moran's I statistic for MERFISH,
675 STOmics and Xenium. **d**, Examples of output files generated by AW workflow with example
676 data from coronal mouse kidney section generated by Visium. **e**, The user interface allows the
677 multiple, co-planar 2D slices to be uploaded in tandem and aligned to form a single data

object for processing. **f**, Multiple, serial Visium slides can be (**f_i**) uploaded in tandem (**f_{ii}**) so they can be combined into a 3D object (**f_{iii}**), demonstrated here with data from the human embryonic heart at 6 dpc .The tissue images are used for reference.

Supplementary Figure 3. VR-Omics architecture. **a**, VR-Omics will accept as input sequencing and imaging-based SRT data of different technologies. **b**, The AW processes, filters and performing spatial analysis and producing output files. **c**, Data can be explored using VR-Omics as a 3D Visualiser in a virtual environment or desktop application as shown here with human embryonic heart at 6 dpc [22]. **d**, Output files, screenshots and video recordings are generated from the Visualiser.

Supplementary Figure 4. Features of the Visualiser. **a**, Gene search. **a_i**, Gene search bar options for visualisation of selected gene expression patterns. **a_{ii}**, Gene expression scale can be visualised with a colour map. The colour map uses a blue to red gradient, with lower expression levels indicated in blue and higher expression levels in red. The image represents the *EPCAM* gene expression in a breast tumour section (Xenium). **a_{ii}**, Binary gene expression can be visualised . **b**, Visualisation of different dimensionality reduction methods, either projected back onto the tissue coordinates or as a UMAP or t-SNE pot. **c**, 3D model overlay. **c_i,** Required inputs. 3D-model can be overlayed over single or multiple SRT slides in the Visualiser then aligned and orientated. **c_{ii},** Example of 3D model overlay displayed with data from the developing human heart. **c_{iii}**, Accepted file formats. **c_{iv}**, Available alignment movements. **d**, Selection of ROIs throughout slices and output. **d_i**, User-defined selection of ROIs within 2D slide with option to select same ROI across serial 3D sections or to select up to 4 ROIs within an object. **d_{ii}**, Visualisation of clusters in MERFISH adult mouse brain and zoomed individual clusters. **e**, Side-by-side comparison. **e_i,** Allows comparison of two different gene profiles

701 within identical copies of the same section for comparison of marker genes. **e_{ii}**, Side-by-side
702 comparison displayed using a Xenium breast tumour section[6]. Expression of *EPCAM* is
703 displayed in the left panel and expression of *ELF3* in the right panel. **f**, After side-by-side
704 comparison has been selected, deselecting this option will ask the user to merge the slides.
705 This creates a comparison of gene expression within the tissue section. Areas with more similar
706 expression between the two genes will be displayed in cool colours, with areas of difference
707 in warm colours, displayed here with the Visium human lymph node.

708 **Supplementary Figure 5.** Additional Visualiser features. **A**, Selection of screenshot function
709 within the Visualiser for export of .png files, displayed here with 3D data from human
710 embryonic heart at 6 dpc. **b**, Within the Visualiser, seamless zoom functionality allows the user
711 to more closely inspect particular areas of the tissue, such as in the MERFISH adult mouse data
712 . **c**, Interactive cluster visualisation within the Visualiser allows the user to visualise individual
713 selected clusters across the tissue.

714 **Supplementary Figure 6**. Additional VR-Omics features. **a**, Example of format supported for
715 custom data upload and example of processing and visualisation. Data from coronal mouse
716 kidney section generated by Visium visualised here. **b**, SVG display. **b_{i},** Statistically significant
717 SVGs will appear in the search blue highlighted in blue and a table containing additional
718 information of all identified SVGs can be accessed in the Visualiser, displayed for the coronal
719 mouse Visium brain slice. **b_{ii}**, Example of additional information related to SVGs identified by
720 Moran's I statistic for Xenium and MERFISH data displayed for Xenium breast tumour section.
721 **c**, Additional demo data availabe within VR-Omics for supported data generation platforms. **d**,
722 Tissue image overlay between spots on slide and H&E stained image of the issue. The opacity
723 of the images can be adjusted for maximise alignment of this data. **e**, After searching and

724 selecting for a gene, a minimum expression threshold can be set to only display spots with a
725 normalised expression above set threshold. Displayed here for Xenium breast tumour section
726 . **e**$_{i}$, scale of expression with cooler colours denoting lower expression and warmer colours
727 denoting higher expression. Displayed here with gene *STC1*. **e**$_{ii}$, Alternatively once the
728 threshold has been set, expression of a gene such as *HARCR2* displayed here, can be displayed
729 in a binary manner as being 'on' or 'off' above the threshold.

730 **Supplementary Figure 7**. Cross-platform comparison of data generated from a mouse brain
731 coronal dataset, all visualised within the VR-Omics framework.

732 **Supplementary Figure 8**. Additional clustering data of cardiac rhabdomyomas. **a,** STAGATE
733 labelled clusters using VR-Omics for analysis of MCHTB361 sample 2. **b,** STAGATE labelled
734 clusters using VR-Omics for analysis of MCHTB361 sample 3**. c,** STAGATE labelled clusters
735 using VR-Omics for analysis of MCHTB361 sample 1. **d**, BayesSpace joint clustering of multi-
736 slice, co-planar MCHTB302 dataset used for orthogonal validation of results generated within
737 VR-Omics. **e**, STAGATE labelled clusters using VR-Omics of multi-slice, co-planar MCHTB362
738 sample 2.

739 **Supplementary Figure 9:** GO analysis of cardiac rhabdomyomas using Metascape. **a**, GO
740 results from MCHTB361 sample 2. **b**, GO results from MCHTB361 sample 3. **c**, GO results from
741 MCHTB362 multi-slice, co-planar dataset sample 2.

742

743

744

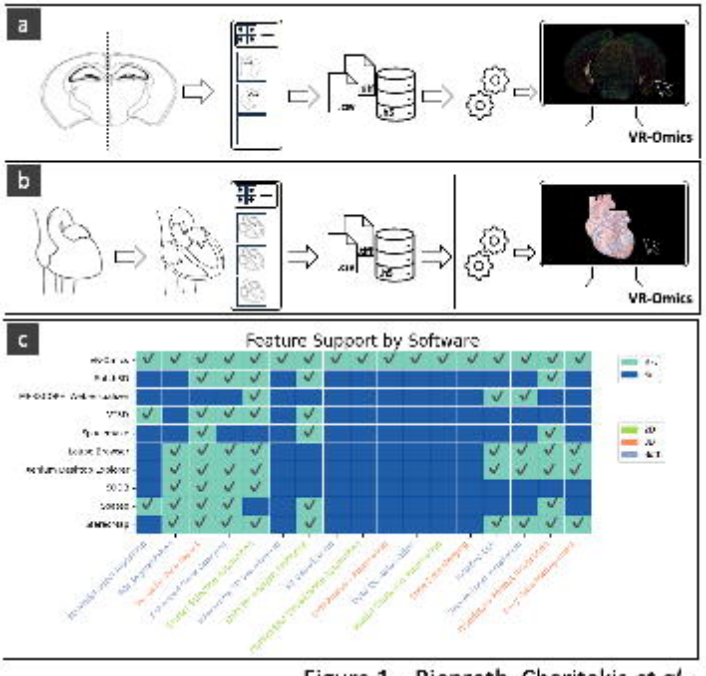

Figure 1 – Bienroth, Charitakis *et al.*

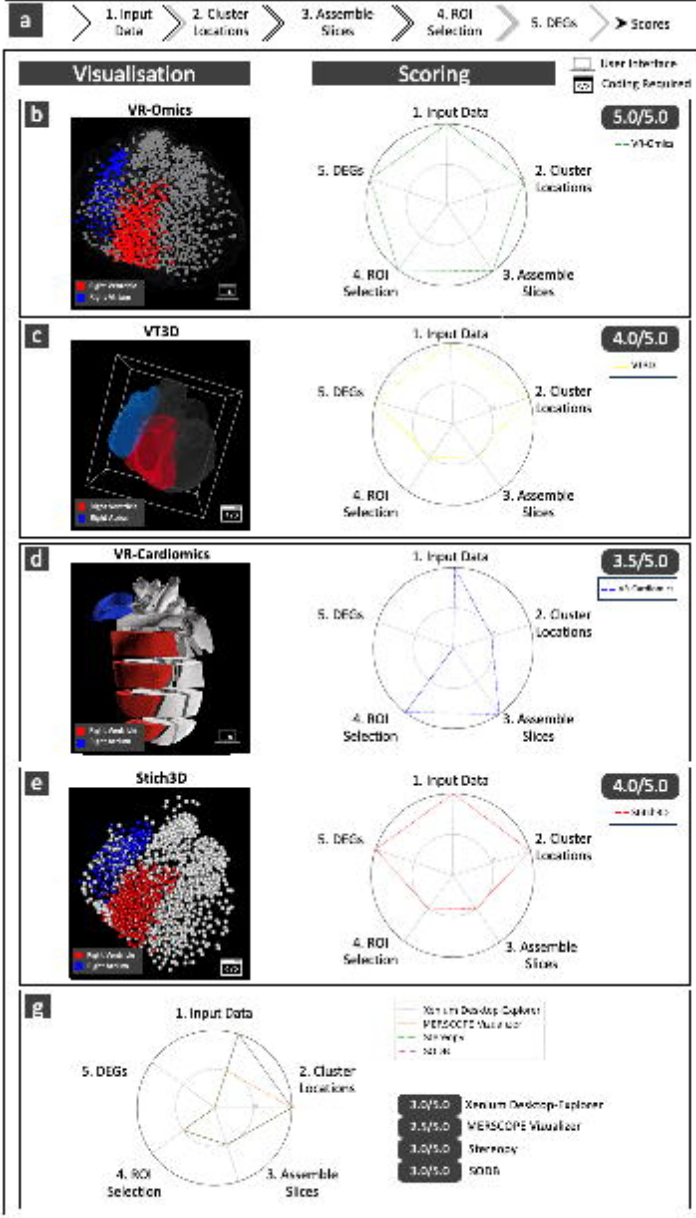

Figure 2 – Bienroth, Charitakis *et al.*

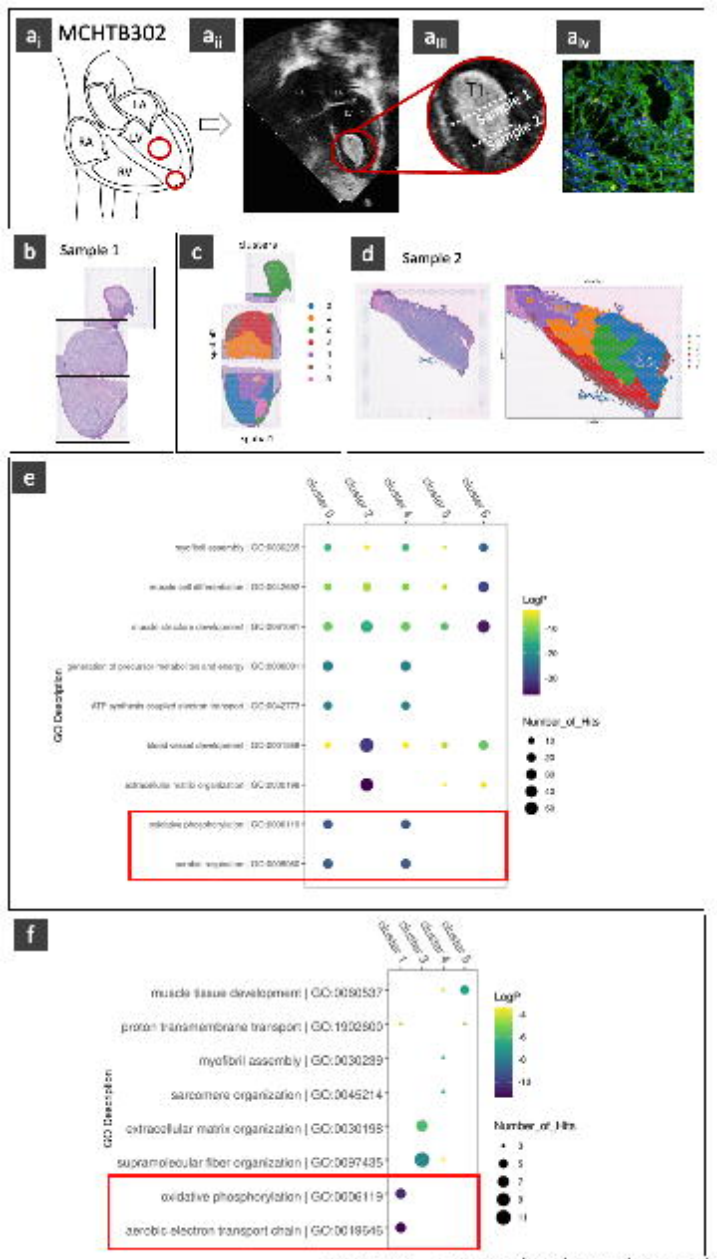

Figure 3 – Bienroth, Charitakis *et al.*

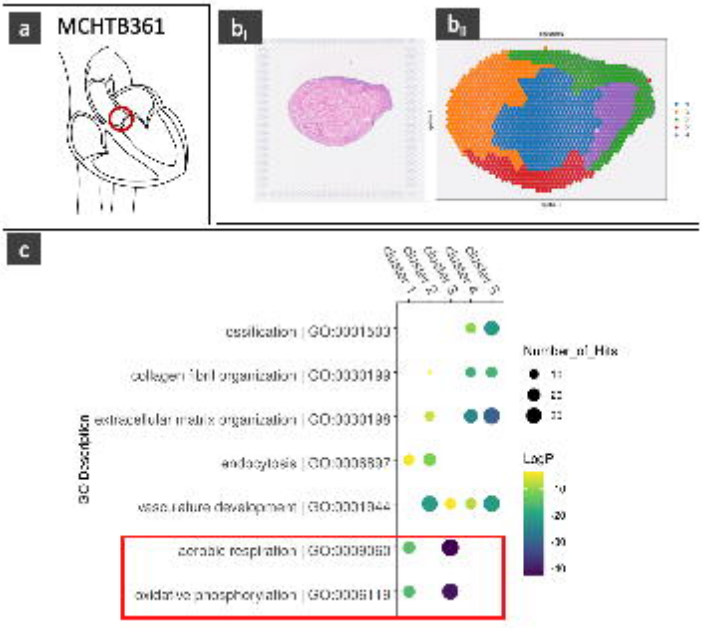

Figure 4 – Bienroth, Charitakis *et al.*

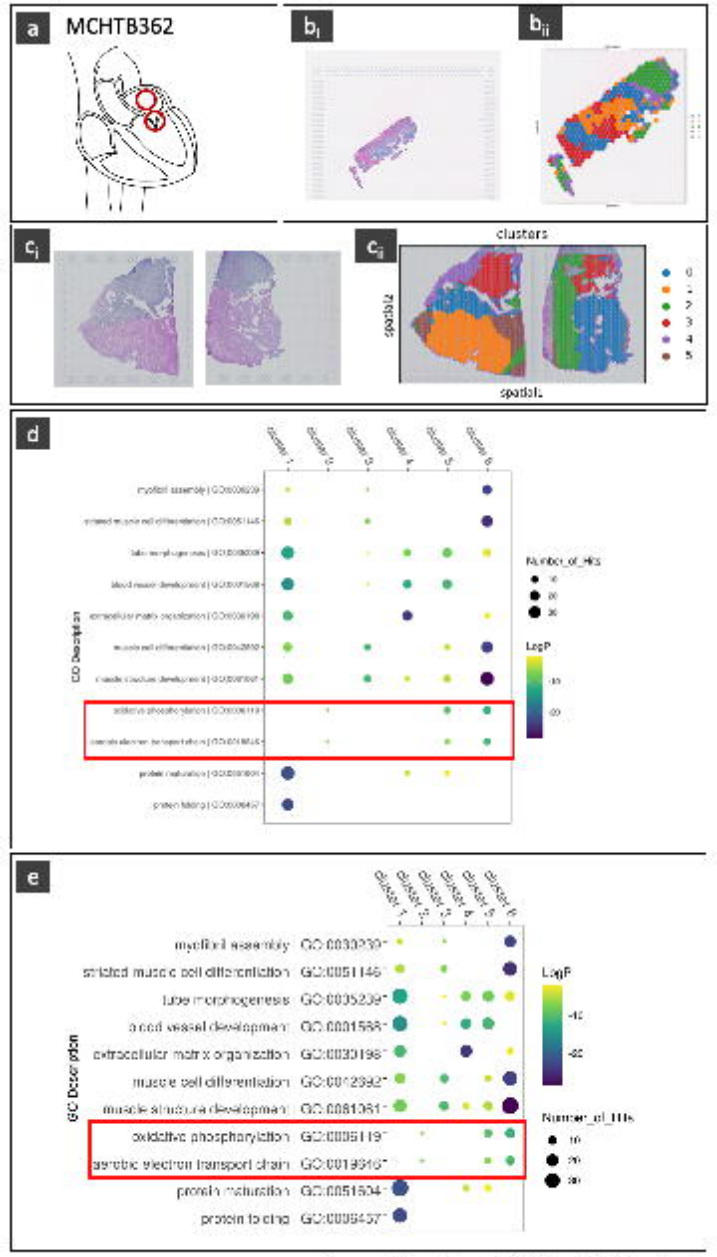

Figure 5 – Bienroth, Charitakis *et al.*